Growth evolution and customized attributes of catalyst-free ZnO nanowires: role of varied Ar/O$_2$ flow rate

H. I. Abdulgafour[1], Naser M. Ahmed[2,*] , Z. Hassan[3], F. K. Yam[2], and A. Sulieman[4]

[1] *Department of Geophysics, College of Remote Sensing and Geophysics, AL-Karkh University for Science, Baghdad 10069, Iraq*

[2] *School of Physics, USM, 11800 Penang, Malaysia*

[3] *Institute of Nano Optoelectronics Research and Technology (INOR), Universiti Sains Malaysia, 11800 USM Penang, Malaysia*

[4] *Radiology and Medical Imaging Department, College of Applied Medical Sciences, Prince Sattam Bin Abdulaziz University, Alkharj, Saudi Arabia*

ABSTRACT

This paper reports a tailored structure, morphology, optical behavior, and growth evolution of catalyst-free ZnO nanostructures (ZONSs) synthesized on quartz substrates using the wet thermal evaporation method. The as-prepared samples were thoroughly characterized to determine the influence of varying rates of Ar and wet O$_2$ gas flow (150, 250, and 350 sccm) on their overall properties. Scanning electron microscopy (SEM) images revealed the formation of high-quality ZONSs of various shapes, including nanowires, aligned nanorods, and nanorods-like tetrapods with different dimensions. X-ray diffraction (XRD) patterns displayed the most intense diffraction peak at (002), which was attributed to the preferred growth orientation and crystallinity of such nanomaterials. Photoluminescence (PL) spectra showed an enhancement in the peak intensity. The position of the ultraviolet emission peak of ZONSs was red-shifted as the gas flow rate increased. Raman spectra exhibited the high-intensity E2 and very weak (suppressed) E1L Raman mode for all samples, indicating the accomplishment of good crystal quality in wurtzite hexagonal crystalline ZONSs of the samples. Furthermore, the optimum flow rate for synthesizing high-density, superior quality, and higher nanocrystalline ZONSs was found to be 350 sccm. This work can contribute toward the development of the production of various nano-optical devices.

Address correspondence to E-mail: nas_tiji@yahoo.com

1 Introduction

The unusual physical and chemical properties of various nanomaterials have attracted researchers' attention in the field of science, technology, and engineering. Recently, various semiconductor nanostructures became interesting mainly due to their unique electrical and optical useful attributes for optoelectronic applications. These nanoscale morphologies incorporate zero-dimensional (0D) nanostructures (quantum specks and nanoparticles), 1D nanostructures, including the nanotubes [1], nanowires [2], nanorods [3], nanobelts [4], nanocables [5], nanoribbons [6], and 2D nanostructures (quantum well and film). These nanostructures have intensively been studied due to their fundamental scientific importance and usefulness in nanoelectronics, nanomechanics, and to their flat panel displays. Being a wide bandgap (3.37 eV) semiconductor, zinc oxide (ZnO) is among the vital technological materials and greatly prospective for shortwavelength optoelectronic devices [7]. The 1D ZnO nanostructures (ZONSs) exhibit many novel properties due to their quantum confinement effect and/or extremely high surface-to-volume ratio. Several techniques, such as chemical vapor deposition (CVD) [8], enhancement of UV photoluminescence in ZnO tubes grown by metal organic chemical vapor deposition (MOCVD) [9], and modeling of the catalyst-free growth process of ZnO nanowires [10] have been employed to synthesize high-quality ZnO films. Besides, the effects of growth conditions on the structural properties of ZONSs deposited on sapphire substrate by metal organic chemical vapor deposition have been studied [11]. Furthermore, various techniques have been successfully employed for the growth of ZnO nanowires. These include chemical or physical vapor deposition, thermal evaporation, magnetron sputtering, and a template-based method. The controlled crystalline size, orientation, and density of nanowires are the vital parameters regarded as the basis for various applications [12]. Chien-Wei Huang et al. have reported the effect of O_2/Ar gas flow ratios on the properties of cathodic vacuum arc deposited ZnO thin films on polyethylene terephthalate substrate [13]. Moreover, Rasheed et al. have also studied the effect of gas sputtering flow rate on the sensitivity of multi-layer (ZnO–Cu–ZnO) extended gate field effect transistor [14]. Despite its facile and economic nature, thermal evaporation technique has not been widely explored. This method could also be utilized to deposit oxides having low melting, decomposition, or sublimation point. More importantly, the quality of different nanostructures can be customized by adjusting the nature and rates of flowing gases and growth temperatures and times.

Based on these advantageous features of the thermal evaporation technique and the ZnO's potentiality, we prepared high-quality ZONS in the absence of any catalysts. Nanostructures with various morphologies, including ZnO nanowires (ZONWs), aligned nanorods (ZONRs), and tetrapod-like nanorods (ZOTNRs) were obtained and characterized at room temperature using various analytical tools. In this process, the flow rate of Ar/O_2 gases was varied to evaluate its influence on the structure, morphology, and the optical characteristics of the as-grown nanostructures. The results were analyzed and discussed. Essential insight on the growth mechanism of these nanostructures was underscored.

2 Materials and methods

2.1 Preparation of ZONSs

The thermal evaporation method (at 800 °C for 60 min) was used to synthesize ZONSs on quartz substrate in which ultrafine Zn powder was evaporated in the absence of any catalysts. Tube furnace (Thermolyne type F-21100) with a 25 mm inner diameter has been applied. The flow rate of Ar/O_2 gases has been varied for controlling the morphology of the studied ZONSs. First, quartz wafers (acted as substrate) were cut into pieces of 1.2×1.2 cm dimension. The substrates were then cleaned (ultrasonically) in acetone and isopropyl alcohol (IPA), and followed by a distilled water rinse. Next, the cleaned wafers were left to dry under nitrogen gas flow. Zn powder (purity 99.99%, Alfa Aesar) was placed in a ceramic (alumina) boat before being quickly positioned at the furnace's center set at a temperature (420 °C). Then the quartz substrate was kept above the source (ceramic boat containing Zn powder) and the temperature of the furnace was increased to 800 °C under different flow rate (150, 250–350 sccm) of highly pure Ar gas and wet O_2. During the growth process, the growth parameters include furnace pressure. In addition, the ratio of the Ar gas and wet

O_2 was used as the carrier gas, and the total gas flow rate for both the Ar gas and wet O_2 in the furnace was fixed at 400 sccm using a mass flow rate controller 100–400 sccm. Then, the reactor flow rate ratio of Ar and wet O_2 was varied from 150 to 350 sccm at 100 sccm intervals. The gas flow should be kept in the laminar flow regime to achieve stable flow in the furnace. For this reason, the furnace pressure used in this work was reduced to achieve a stable flow and reduce the pre-reaction. The three nanostructured samples were prepared and designated as ZONS150, ZONS250, and ZONS350.

2.2 Characterizations techniques

The as-grown ZONSs were characterized at room temperature. The surface morphology and microstructures of the prepared ZONSs were studied using SEM, JOEL JSM-6460-LV. The SEM measurements for the surface morphological studies were achieved at (10 kV), while the crystalline structure of the suggested ZONSs was estimated using a high-resolution X-ray diffraction (HR-XRD) machine, PANalytical X'pert Pro MRD. A Cu–Kα_1 source of radiation ($\lambda = 1.5406$ Å) was utilized to assess the crystalline quality and the phase identification. Furthermore, the optical properties of the as-grown ZONSs were investigated at 25 °C using photoluminescence (PL) and Raman scattering techniques. The investigation was achieved using Jobin Yvon HR800-UV Raman spectrometer equipped with helium cadmium (He–Cd) laser (325 nm). The argon ion laser (514.5 nm) was also utilized as the excitation source for the PL and the Raman measurements at room temperature. Moreover, the incident laser power for the two measurements was 20 mW. Finally, the thickness of the nanostructured films was estimated using as the optical reflectometer, Filmetrics F-20.

3 Results and discussion

3.1 SEM analysis

Figure 1 shows the SEM images for all the samples prepared at different flow rates of the gases. Sample grown at 150 sccm (Fig. 1a) revealed dense ZONWs with diameters ranging between 50 and 70 mm and a length of more than 5 µm. The sample grown at 250

sccm (Fig. 1b) displayed nucleation of strongly aligned ZONRs of diameters ranging from 100 to 130 nm and a length of about 2 µm. Furthermore, the sample grown at 350 sccm (Fig. 1c) disclosed the existence of weakly aligned ZOTNRs of diameters ranging from 120 to 150 nm and a length of 3.5 µm. The average diameters of the grown NWs/NRs were found to increase with the rise in the flow rates of Ar/wet O_2 gases. It could be observed that the microstructures and morphologies of ZONSs were appreciably influenced by the partial pressure of the vapor phase and the gas flow rates. As such, it was affirmed that the morphologies of the proposed ZONSs could be desirably controlled by regulating the flow rates of gas mixture (Ar + wet O_2).

It is worth mentioning that the possession of rough surface morphology (shape, size, and geometry) in the achieved ZONSs could play a significant role in controlling their formation at the initial stage related to the growth evolution. The observed shortening in lengths and widening in diameters with the increase in gas flow rate is attributed to the rough surface morphologies of the ZONSs [15]. This evolution in the morphology of ZONSs was majorly ascribed to the mechanism of surface diffusion. It is known that for a bulk crystalline system, the surface energy minimization acts as the driving force for the progression of crystallinity. At equilibrium, a self-texture is exhibited in the absence of any impact of epitaxy between the film and the substrate. Therefore, the film grows along the crystallographic plane parallel to the surface, having minimum free energy (the plane with the closest packing of atoms and the maximum reticular density) [16]. Finely, the growth rate decreased with increasing furnace pressure because the thickness of the boundary layer increased with increasing furnace pressure. The thicker the boundary layer, the harder the diffusion of atoms into the growing surface. By reducing the furnace pressure, the gas flows on the sample surface became more stable. The diffusivities of these gases increased with decreasing chamber pressure and therefore the growth rate increases [11]. The gas phase reaction causes the generation of particles and results in a high surface roughness of the sample. The gas flow should be kept in the laminar flow regime to achieve stable flow in the chamber. For this reason, the chamber pressure used in this work was reduced in order to achieve a stable flow and reduce the pre-reaction [11].

Fig. 1 SEM micrographs for ZONSs samples prepared at different flow rate of gases: **a** 150 sccm, **b** 250 sccm, **c** 350 sccm
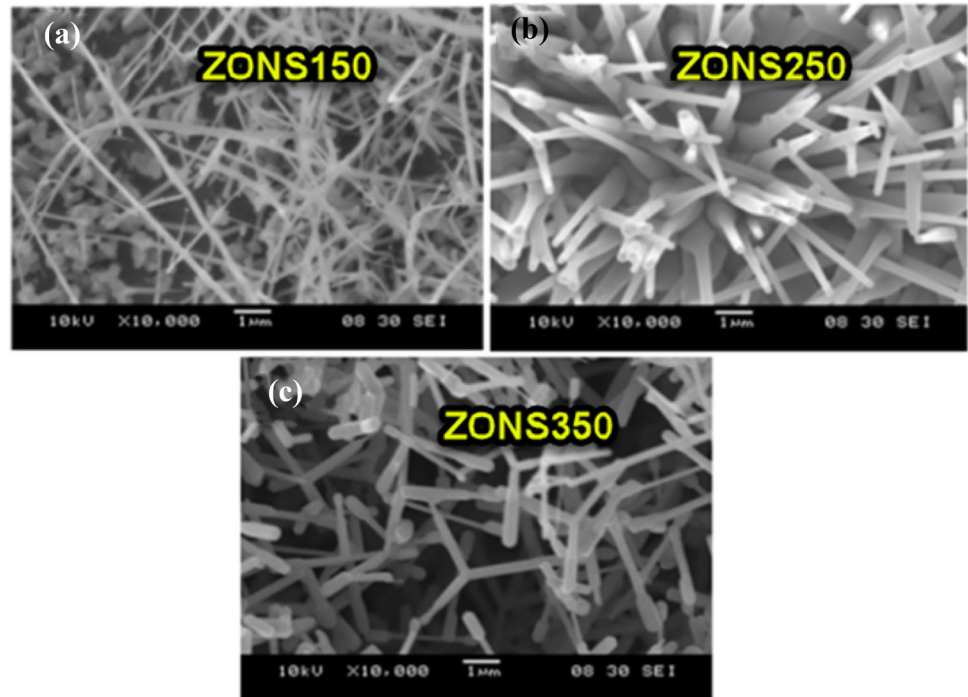
3.2 XRD characterization

Figure 2 displays the gas flow rate-dependent XRD pattern of the as-synthesized ZONSs, which comprises few characteristic sharp peaks assigned to the high-purity nanocrystalline phases ZnO. All
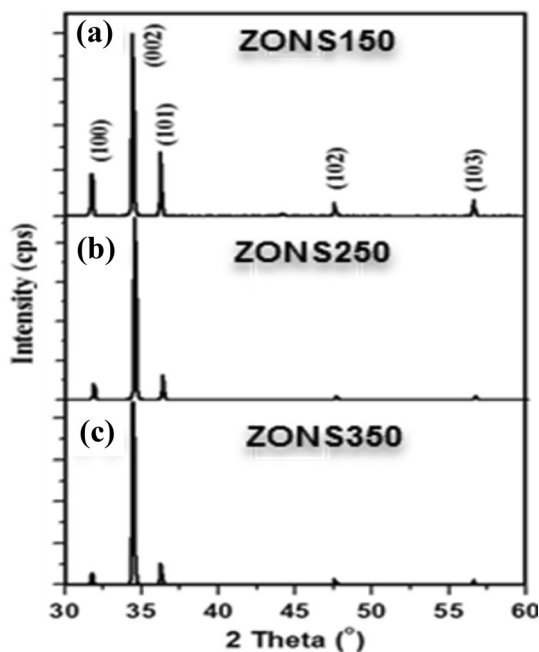

Fig. 2 XRD patterns for ZONSs samples prepared at different flow rate of gases: **a** 150 sccm, **b** 250 sccm, **c** 350 sccm

observed diffraction peaks have been indexed to wurtzite (hexagonal) structure related to ZnO lattice (JCPDS card, No. 80-0074), in the absence of any impurity phase. The observed diffraction peaks of ZONSs (100), (002), and (110) corresponded to the wurtzite (hexagonal) crystal structure of the ZnO lattice planer orientations. For all the samples, the appearance of an intense diffraction peak at (002) is due to the preferred growth orientation of ZONSs along the crystallographic c-axis (perpendicular to the substrate) of ZnO lattice. Additionally, the ZONS 350 sample grown at the gas flow rate of 350 sccm depicted higher (002) peak intensity, which indicates its higher crystallinity. Thus, the flow rate has a significant effect on the crystallinity of ZONS which involved the mechanism of nucleation and growth.

The XRD data were further analyzed to evaluate the lattice parameters (a and c) and the average grain size (D) of grown ZnO nanocrystallites with different morphologies. The most intense (002) peak was used in this regard. Scherrer formula $D = k\lambda/(\beta \cos\theta)$ was used for the evaluation [17]. Where k represents a constant, equal to 0.90, λ represents the incident X-ray wavelength, and β represents the full width at half maximum (FWHM) of the intense XRD peak. The average value of D was about 30.2, 38.4, and 40.5 nm for the ZONSs grown at the gas flow rates of 150, 250, and 350 sccm, respectively. It could be observed that

the values of D increased with the increase in the gas flow rate. The (002) diffraction peak position of the deposited ZONSs was shifted to higher angles from 34.4278° to 34.4694° with the increase in the gas flow rates from 150 to 350 sccm.

As shown in Fig 3, the values of a, c and D attained maximum at 350 sccm. The attainment of slightly higher values of the lattice parameter c for all the samples (Table 1) compared to the bulk ZnO value (0.52065 nm) could be attributed to the existence of tensile lattice strain in the film containing ZONWs, ZONRs, and ZOTNRs. Furthermore, the strain was discovered to be enhanced by increasing the flow rate. This result is in agreement with a previous report wherein the ZnO films grown at different flow rates were shown to possess a compressive strain [18]. Likewise, the observed shift in the diffraction peak position toward higher angles with the increase in the gas flow rates suggested the generation of residual compressive stresses in the as-grown films containing ZONSs. Tsao et al. have also acknowledged the diffraction peak position shift toward a higher angle with the enlargement of grain diameter in ZONSs [19]. A positive mismatch in the lattice parameters of ZONSs produced a tensile strain, while a negative mismatch generated a compressive strain. Consequently, these strains created residual stresses in the crystal lattice as well as at the substrate interface. With the increase in film thickness at higher flow rates, the degree of tensile strain was also increased which in turn extended the lattice parameters a and c as well as enlargement of D.

3.3 PL spectra

The peak intensity (Fig. 4) was enhanced, and the position of the UV emission peak of the as-prepared ZONSs was red-shifted (toward higher wavelength) with the increase in gas flow rate. The appearance of a relatively sharper peak at a lower wavelength (in the range of (272–388 nm) has been attributed to the near band-edge emission (NBE) while the broader visible one (518–520 nm) is due to the deep-level emission (DLE). The NBE UV emission transition was due to the recombination of free excitons via exciton–exciton collision [20, 21].

The lowest intensity of the green emission peak (at 520 nm) is observed for the sample grown at 350 sccm. There is no consensus about the exact origin of the green emission, although it is believed that this peak originates because of electronic transitions from shallow donors states to the Zn vacancies [22]. Furthermore, some researchers related the origin of this green emission peak to the occurrences of native point defects like the zinc vacancies (V_{Zn}) or oxygen vacancies (V_O) [23]. As mentioned, by adjusting the gas flow rates the concentration values of the Zn and O vapors may be controlled; therefore, the zinc and oxygen vacancies can be manipulated to get PL intensity enhancement through the customization of growth morphology [24]. Thus, the optical bandgap of the ZONSs can be tuned, which is a useful parameter for the optoelectronic devices. Above all, the PL spectral peak position can be modified by adjusting the gas flow rate. The value of FWHM of the NBE PL peak was enlarged from 18.3 to 38.7 nm
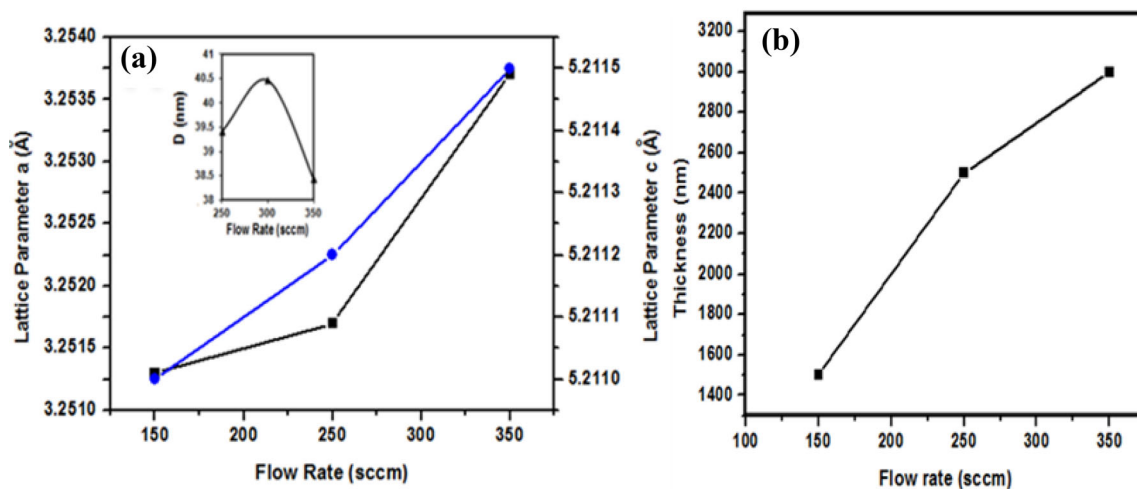

Fig. 3 Gas flow rate-dependent variation for the lattice parameters and the thickness of the nanostructured thin films, respectively

Table 1 Estimated values of *a*, *c*, *D*, the intense (002) XRD peak position and the thickness of the film containing ZONSs

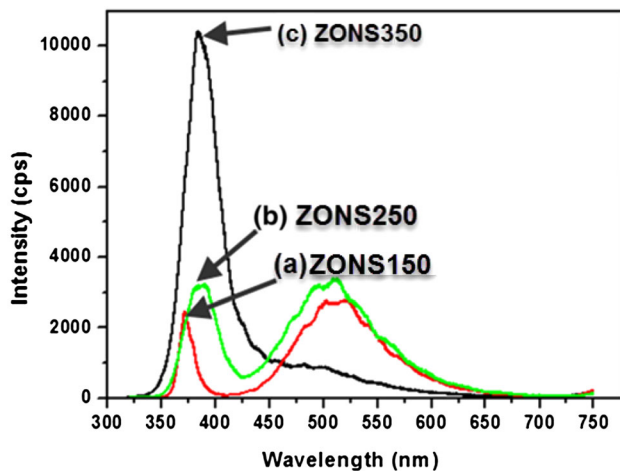| Samples	(002) peak position (°)	*a* (Å)	*c* (Å)	*D* (nm)	Film thickness (μm)
ZONS150	34.4278	3.2513	5.2110	30.2	1.2
ZONS250	34.4546	3.2517	5.2112	38.4	2.5
ZONS350	34.4694	3.2537	5.2115	40.5	3.4

Fig. 4 Gas flow rate-dependent recorded PL spectra of the ZONSs, which consisted of two broad peaks

when the gas flow rate was increased from 150 to 350 sccm (Table 2). This observation was majorly attributed to the effects of strong quantum confinement and improvement in the crystallinity of the proposed ZONSs.

The observed red-shift in the NBE peak position was attributed to the effect of tensile strain in the nanostructured film (Table 2). Generally, the ratio of UV to DLE peak intensity is regarded as the major factor for comparing the alteration in the optical properties among different ZONSs deposited with varied gas flow rates. The ratios were 1:0.7, 1:1.2, and 1:13.1 for the samples deposited at the gas flow rates of 150, 250, and 350 sccm. Meanwhile, the achieved optical quality of the ZOTNRs grown at a flow rate of 350 sccm was higher (no defects and vacancies as

Table 2 NBE PL spectral peak position of all the ZONSs grown at different gas flow rate

Sample	NBE peak position (nm)	FWHM (nm)	Peak shift (nm)
ZONS150	372.3	18.3	4.2
ZONS250	387.8	34.2	19.8
ZONS350	385.5	38.7	17.5

well as a complete absence of green emission peak) compared to ZONWs and ZONRs deposited at lower gas flow rates. The realization of high-quality ZONSs over the wide area indicated their effectiveness in optoelectronic applications.

The obtained PL peak shift and broadening in the FWHM indicate a widening in the optical bandgap, hence, reduction in the nanocrystallite size. The higher shift in the PL peak position was attributed to the effect of charge carrier quantum confinement. It indicated the stronger confinement of nanocrystallites in lower dimensional structures, causing a higher recombination probability of electrons and holes. Consequently, the emission efficiency was enhanced, and physical properties were improved due to the lowering in the dimension of ZONSs and evolution in the morphology. In general, when the nanosystem size becomes larger than a certain characteristic length scale its properties approach to that of the bulk counterpart. Conversely, when the system size is smaller than or comparable to a characteristic length scale, its properties are decided by the nature of quantum confinement, morphology, and surface states [25, 26].

3.4 Raman spectra

The Raman data were used to determine the presence of various bonding vibrations (phonon modes from the functional groups), crystal perfection, and structural defects. The wurtzite-type ZnO belonged to space group symmetry of C^4(P63mc) with 2 formula units in primitive cell. Raman spectra are highly sensitive to crystal quality and structural defects. The disorders related to grown products have been evaluated by the nature of detected phonon modes.

With a wurtzite hexagonal structure, ZnO belongs to the C_{6V}^4 space group and 8 sets of the optical phonon modes at Γ symmetry point in Brillouin zone are categorized as $A_1 + 2B_1 + E_1 + 2E_2$ modes (Raman active), $2B_1$ modes (Raman silent), and $A_1 + E_1$ modes (infra-red active). The E_1 mode being a polar mode was split into two branches called transverse

optical (TO) and longitudinal optical (LO) modes [27].

The observed characteristic peaks of the wurtzite ZnO hexagonal phase were assigned (Fig. 5) to the E_2H–E_2L, A_1(TO), E_1(TO), E_2H, A_1(LO) and E_1(LO) [28]. As shown in (Table 3), the low-frequency mode E_2 (Low) that generally appears at 101 cm^{-1} due to the Zn sublattice vibration was not observed, whereas high-frequency mode E_2 (high) involving vibrations of oxygen atoms only as evidenced [29]. Furthermore, the induced stress in the wurtzite crystal could affect the E_2 phonon frequency, an indicator of stress induced vibration in the lattice. The obtained increment or decrement in the E_2 phonon frequency is due to compressive or tensile stress in the lattice of ZONSs. The occurrence of sharp, strong, and dominant E_2 (high) peak centered at

438.2, 438.5, and 439.3 cm^{-1} corresponding to the ZONS150, ZONS250, and ZONS350 samples clearly indicated intrinsic characteristic phonon vibration of the Raman active mode in wurtzite hexagonal ZnO crystal [30]. Irrespective of the gas flow rates, the peak of E_2H mode in the present ZONSs revealed a blue shift compared to the bulk ZnO value of 437 cm^{-1} [29], which was attributed to the effects of optical phonon confinement, laser induced heating, and/or defects/impurities assisted phonon localization in the nanostructures. Additionally, anisotropic internal strains which correspond to different directions of growth might have also contributed to this blue shift, and these results are in accordance with the presented XRD data.

The presence of the high-intensity E_2 and very weak (suppressed) E_1L Raman mode for all the samples

Fig. 5 Gas flow rate-dependent Raman spectra (under the argon ion laser excitation of wavelength 514.5 nm) of the synthesized ZONSs
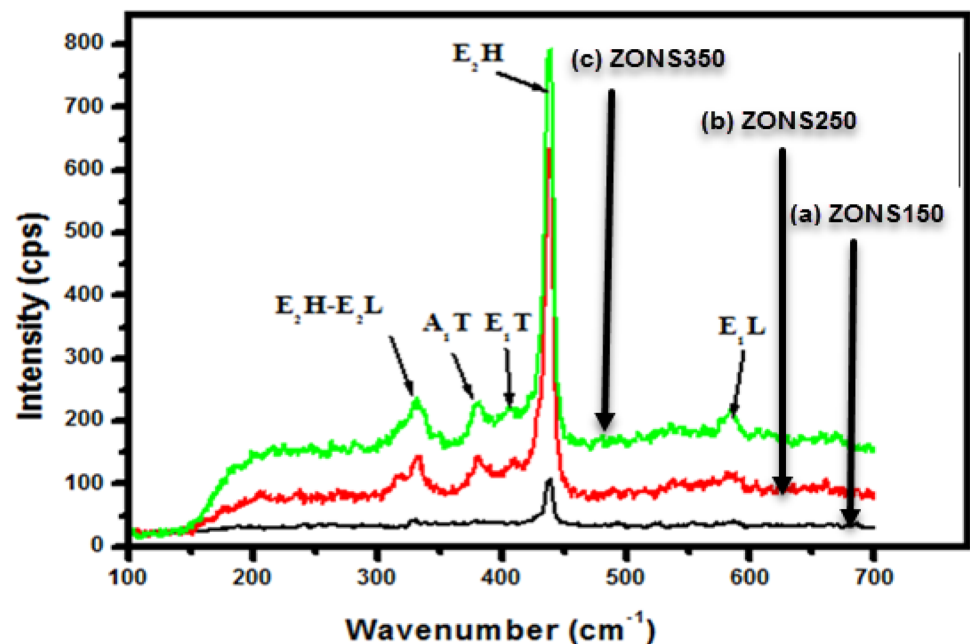
Table 3 Flow rate-dependent Raman peak position and the intensity of the as-grown ZONSs

Samples	Assignments of peaks	E_1(LO)	A_1(TO)	E_1(TO)	E_2H	Peak shift of E_2H (cm^{-1})
ZONS150	Peak position (cm^{-1})	583.5	379.4	409.4	438.2	1.2
	Intensity (a.u.)	40	40.11	38.8	107.295	
ZONS250	Peak position (cm^{-1})	582.6	381.6	410.5	438.5	1.5
	Intensity (a.u.)	120.5	144.5	141.5	635.422	
ZONS350	Peak position (cm^{-1})	583.6	382.144	411.061	439.3	2.3
	Intensity (a.u.)	219.6	231.5	222.5	791.622	

indicated the accomplishment of good crystal quality in wurtzite hexagonal crystalline ZONSs. In general, it is accepted that the existence of E_1(LO) mode has been associated with the formation of defects in ZnO. Consequently, detected E_1(LO) peak at 583.5, 582.6, and 583.6 cm^{-1} for ZONS150, ZONS250, and ZONS350, respectively, indicated its emergence due to the existence of defects from O vacancies, Zn interstitials or their complexes and free carriers [31]. This observation in sequence could support the disclosure of the defect level-induced visible PL emission band of the produced ZONSs. In short, all these factors controlled by the gas flow rates could appreciably influence the optical properties of the grown ZONSs. Meanwhile, the revelation of the three weak Raman peaks centered at 330, 410, and 381.5 cm^{-1} related to E_2H–E_2L, E_1(TO), and A_1(TO)modes, respectively, could be attributed to the multiphoton scattering process in the grown ZONSs [32]. However, these modes were utterly absent in ZONS150 sample.

The structural properties of ZONSs obtained from the Raman spectral analyses were supported by the XRD and SEM results. The intensity of E_2H peak for ZONS350 sample containing ZOTNRs is reasonably higher compared to the other samples. This indicates an improved degree of crystallization in the former [33]. In fact, the PL spectral analyses also showed higher crystallinity in the sample containing ZOTNRs (prepared at 350 sccm) than the one containing ZONWs (at 150 sccm) and ZONRs (at 250 sccm). Besides, the observed blue shift in the E_2H Raman peak (from 1.2 to 2.3 cm^{-1}) in the present ZONSs (compared to the bulk ZnO) with the increase in gas flow rate (from 150 to 350 sccm) clearly verified the presence of compressive stress and defects in the ZnO film containing diverse morphologies. The stimulation of maximum and minimum compressive stress effects in the ZONSs was characterized by the observed slight shifts in the UV PL emission peak. This compressive stress was mainly originated from the lattice mismatch between the substrate and ZONSs.

The Raman spectra were accompanied by a strong luminescence emission background corresponding to green wavelength. The green PL emission from ZONSs was originated from the above bandgap excitation. According to Vanheusden et al., this visible emission can be due to recombination of the electrons in signally occupied oxygen vacancies with photoexcited holes in valence band [34]. Even though the nature of green PL emission remains controversial, it has been majorly verified that the oxygen vacancies have been causing emission. Alternatively, the presence of many intrinsic and surface defects in ZONSs may lead to the distribution of the levels of the surface energy, which forms the surface energy band. Consequently, the sub-bandgap excitation at 488 nm can induce the excitation of surface states thus producing the green PL emission [22]. In short, the morphology and the growth evolution in the ZONSs are correlated to their optical behaviors.

4 Conclusion

The high-quality ZONSs with various morphologies such as NWs, aligned NRs, and TNRs were deposited on quartz substrates by a simple thermal evaporation approach devoid of any catalyst. The Ar/wet O2 gas flow rate was varied from 150 to 350 sccm at the growth temperature of 800 °C. The impact of altering gas flow rates on the growth evolution, structure, surface morphology, and PL emission characteristics of deposited ZONSs was examined. It was shown that the partial pressure of wet oxygen played a vital role in the growth mechanism of wurtzite hexagonal ZONSs wherein the nucleated Zn droplets from the vapor phase initiated the growth. The diameters of the ZONWs/ZONRs were increased and the lengths were shortened with the increase in the gas flow rate. Compared to the ZONWs deposited at a lower flow rate of 150 sccm, the ZONRs and ZOTNRs grown at a higher flow rate achieved better crystal quality in terms of crystallinity, density, and structural compactness. The PL and Raman spectral analyses of the obtained ZONSs exhibited high optical efficiency and crystallinity. Fundamental insight into the gas flow rate-induced growth mechanism of ZONSs was presented. Thus, the proposed ZONSs film containing varied morphologies may contribute toward the development of efficient optoelectronic devices including ultraviolet lasers and gas sensors.

Data availability

Data and materials are available.

Code availability

Not applicable.

Compliance with ethical standards

Conflict of interest The authors report no conflicts of interest. The authors alone are responsible for the content and writing of this article.

References

1. P. Samadipakchin, H.R. Mortaheb, A. Zolfaghari, ZnO nanotubes: preparation and photocatalytic performance evaluation. J. Photochem. Photobiol. **337**, 91–99 (2017)
2. W.A. Bhutto et al., Controlled growth of zinc oxide nanowire arrays by chemical vapor deposition (CVD) method. Int. J. Comput. Net. Secur. **19**, 135 (2019)
3. N.G. Elfadill et al., Ultraviolet–visible photo-response of p-Cu2O/n-ZnO heterojunction prepared on flexible (PET) substrate. Mater. Chem. Phys. **156**, 54–60 (2015)
4. O.W. Kennedy et al., MBE growth and morphology control of ZnO nanobelts with polar axis perpendicular to growth direction. Mater. Lett. **212**, 51–53 (2018)
5. P. Zhang et al., Pt/ZnO@ C nanocable with dual-enhanced photocatalytic performance and superior photostability. Langmuir **33**, 4452–4460 (2017)
6. C.S. Garoufalis et al., Optical properties of zig-zag and armchair ZnO colloidal nanoribbons. Chem. Phys. Lett. **732**, 136659 (2019)
7. S. Vyas, A short review on properties and applications of ZnO based thin film and devices. Johnson. Matthey. Technol. Rev. (2019). https://doi.org/10.1595/205651320x15694993568524
8. Q. Zhang, C. Li, TiO2 coated ZnO nanorods by mist chemical vapor deposition for application as photoanodes for dye-sensitized solar cells. Nanomaterials. **9**, 1339 (2019)
9. S. Iwan et al., Enhancement of UV photoluminescence in ZnO tubes grown by metal organic chemical vapour deposition (MOCVD). Vacuum **155**, 408–411 (2018)
10. K. Xiangcheng, W. Chuang et al., Modeling of catalyst-free growth process of ZnO nanowires. J. Procedia Manuf. **26**, 49–358 (2018)
11. C.C. Wu, D.S. Wuu, P.R. Lin, T.N. Chen, R.H. Horng, Effects of growth conditions on structural properties of ZnO nanostructures on sapphire substrate by metal-organic chemical vapor deposition. Nanoscale. Res. Lett. **4**, 377–384 (2009)
12. K.H. Kim, K. Utashiro, Y. Abe, M. Kawamura, Growth of zinc oxide nanorods using various seed layer annealing temperatures and substrate materials. Int. J. Electrochem. Sci. **9**, 2080–2089 (2014)
13. H.S. Rasheed, N.M. Ahmed, M.Z. Matjafri, E.A. Kabaa, Ar gas flow rate influnence on the structure properties and electrical behavior of new sensing membrane zno/cu/zno (zcz) extended gate field effect transistor (EG-FET). Dig. J. Nanomater. Bios. **12**(4), 1119–1126 (2017)
14. R.-Y. Chien-W Huang, C.-T. Yang, M.-H. Weng, Effect of O2/Ar gas flow ratios on properties of cathodic vacuum arc deposited ZnO thin films on polyethylene terephthalate substrate. J. Nanomater. (2016). https://doi.org/10.1155/2016/6479812
15. H. Abdulgafour et al., ZnO nanocoral reef grown on porous silicon substrates without catalyst. J. Alloys Compd. **509**, 5627–5630 (2011)
16. C. Ye et al., Zinc oxide nanostructures: morphology derivation and evolution. J. Phy. Chem. B. **109**, 19758–19765 (2005)
17. I. Boukhoubza et al., Morphological and structural properties of ZnO nanorods coated with graphene derivative fabricated by hydrothermal method. J. Phys. Conf. Series (2019). https://doi.org/10.1088/1742-6596/1292/1/012012
18. S. Seo, H. Kang, Strain evolution in heteroepitaxial ZnO/sapphire (0001) thin films grown by radio frequency magnetron sputtering. Thin Solid Films **518**, 6446–6450 (2010)

19. F.C. Tsao et al., Residual strain in ZnO nanowires grown by catalyst-free chemical vapor deposition on GaN/sapphire (0001). Appl. Phys. Lett. **92**, 203110–203113 (2008)

20. S. Alamdari et al., Preparation and characterization of GO-ZnO nanocomposite for UV detection application. Opt. Mater. **92**, 243–250 (2019)

21. H.-S. Chou et al., Temperature-dependent ultraviolet photoluminescence in hierarchical Zn, ZnO and ZnO/Zn nanostructures. Nanoscale **11**, 13385–13396 (2019)

22. A.J. Raghavendra et al., Three-photon imaging using defect-induced photoluminescence in biocompatible ZnO nanoparticles. Int. J. Nanomed. **13**, 4283 (2018)

23. J.L. Lyons et al., First-principles calculations of optical transitions at native defects and impurities in ZnO. Oxide. Mater. Devices IX. (2018). https://doi.org/10.1117/12.2303687

24. D. Zhao et al., Stress and its effect on optical properties of GaN epilayers grown on Si (111), 6H-SiC (0001), and c-plane sapphire. Appl. Phys. Lett. **83**, 677–683 (2003)

25. K. Bajaj, Use of excitons in materials characterization of semiconductor system. Mater. Sci. Eng. **34**, 59–120 (2001)

26. M.S. Gudiksen, J. Wang, C.M. Lieber, Size-dependent photoluminescence from single indium phosphide nanowires. J. Phys. Chem. B **106**, 4036–4039 (2002)

27. X.-H. Zhang et al., Rational design and fabrication of ZnO nanotubes from nanowire templates in a microwave plasma system. J. Phys. Chem. B **107**, 10114–10118 (2003)

28. H. Fukushima et al., Evaluation of oxygen vacancies in ZnO single crystals and powders by micro-Raman spectroscopy. J. Ceram. Soc. Jpn. **125**, 445–448 (2017)

29. T.C. Damen, S. Porto, B. Tell, Raman effect in zinc oxide. Phys. Rev. **142**, 570–574 (1966)

30. A. Khan et al., Catalyst-free synthesis and luminescence of aligned ZnO nanorods. Physica E **39**, 258–261 (2007)

31. F. Decremps et al., High-pressure Raman spectroscopy study of wurtzite ZnO. Phys. Rev. B **65**, 092101–92104 (2002)

32. H. Abdulgafour et al., Growth of zinc oxide nanoflowers by thermal evaporation method. Physica B **405**, 2570–2572 (2010)

33. S. Mandal et al., Temperature dependent photoluminescence characteristics of nanocrystalline ZnO films grown by sol–gel technique. Thin Solid Films **516**, 8702–8706 (2008)

34. K. Vanheusden et al., Mechanisms behind green photoluminescence in ZnO phosphor powders. J. Appl. Phys. **79**, 7983–7990 (1996)